Available online at www.CivileJournal.org

Civil Engineering Journal

(E-ISSN: 2476-3055; ISSN: 2676-6957)

Vol. 10, No. 05, May, 2024

Ultimate Strength of Internal Ring-Reinforced KT Joints Under Brace Axial Compression

Adnan Rasul [1*], Saravanan Karuppanan [1], Veeradasan Perumal [1], Mark Ovinis [2], Mohsin Iqbal [1]

[1] *Department of Mechanical Engineering, Universiti Teknologi PETRONAS, Seri Iskandar 32610, Malaysia.*

[2] *School of Engineering and the Built Environment, Birmingham City University, Birmingham, United Kingdom.*

Received 07 January 2024; Revised 11 April 2024; Accepted 18 April 2024; Published 01 May 2024

Abstract

Internal ring stiffeners are frequently used to improve the ultimate strength of tubular joints in offshore structures. However, there is a noticeable absence of specific design guidance regarding the assessment of their ultimate strengths in prominent offshore codes and design guides. No equations are available to determine the ultimate strength of internal ring-reinforced KT joints. This work developed equations to determine the ultimate strength and the strength ratio of internal ring-reinforced KT joints based on numerical models and parametric studies comprising ring parameters and joint parameters. Specifically, a finite element model and a response surface approach with eight parameters (λ, δ, ψ, ζ, θ, τ, γ, and β) as inputs and two outputs (ultimate strength and the strength ratio) were evaluated since efficient response surface methodology has been proven to give precise and comprehensive predictions. KT-joint with parameters λ=0.9111, δ=0.2, ψ=0.7030, ζ=0.3, θ=45°, τ=0.90, γ=16.25, and β=0.6 has the maximum ultimate strength, and the KT-joint with parameters: λ=1, δ=0.2, ψ=0.8, ζ=0.5697, θ=45°, τ=0.61, γ=24, and β=0.41 has the maximum strength ratio. The KT-joints with the optimized parameters were validated through finite element analysis. The percentage difference was less than 1.7%, indicating the applicability and high accuracy of the response surface methodology.

Keywords: KT-Joint; Response Surface Methodology; Ultimate Strength; Ring-Stiffeners; Initial Stiffness; Optimization; Finite Element Analysis; Strength Ratio.

1. Introduction

Jacket-type offshore platforms are created from circular hollow sections (CHS) tubular segments by welding one end of the branching component (brace) to the main structure (chord), creating tubular joints. A KT joint is among the most commonly employed tubular joints. It has three circular braces welded to the main chord, with the central brace at 90° to the chord and the outer inclined braces at an angle Θ to the main chord, as shown in Figure 1.

Offshore structures are subjected to various complex environmental loads such as earthquakes, ice and mud, ice and waves, buoyancy, and storms [1, 2]. Structural failure can happen when a given structure cannot withstand the applied stresses or forces. Various methods have been employed in the industry to enhance the ultimate strength of tubular joints [3]. Collar and doubler plates [4–12], FRP reinforcement [13–16], and internal rings [17–20] are some of the options available for strengthening. Concrete filling [21], hybrid grouting [22], and hybrid FRP-concrete tubular joints [23] have also been used for the strength enhancement of offshore structures. These alternatives are commonly utilized when the

* Corresponding author: adnan_22006634@utp.edu.my

http://dx.doi.org/10.28991/CEJ-2024-010-05-012

joint's strength is inadequate during development. Internal rings joined inside the chord have numerous advantages over other strengthening techniques, as these substantially improve load-bearing ability, reduce stress concentration factors, increase fatigue life, and prevent wave forces and corrosive attacks [24]. These are called internal rings or stiffeners, as shown in Figure 1.

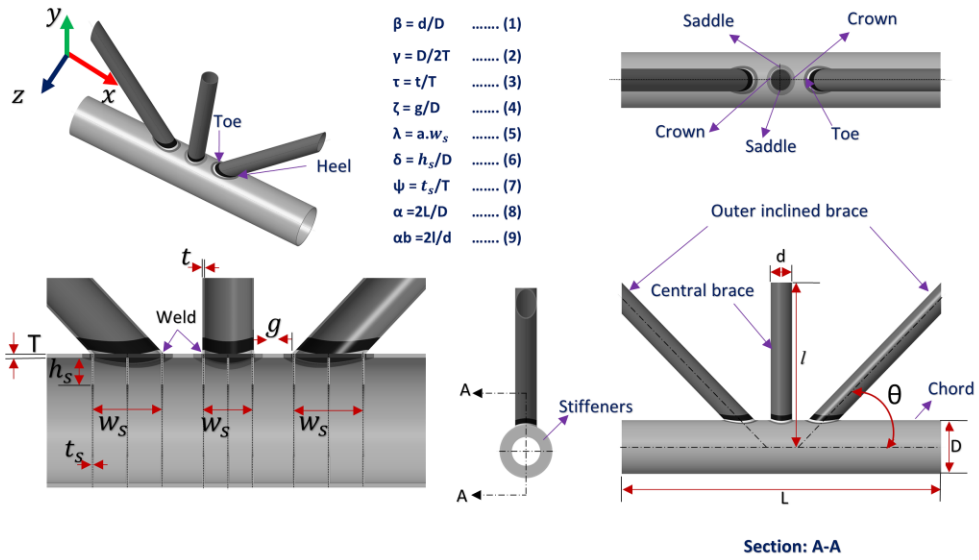

Figure 1. Geometrical notation of internal ring-reinforced KT joints

Internal rings have been shown to increase strength. Lee and Llewelyn-Parry [19] analyzed 42 internal ring-stiffened T-joints and concluded that the internal rings could significantly increase ultimate strength by at least 50% up to 140%. Lee and Llewelyn-Parry [18] generated a theoretical framework to evaluate the structural strength of internally ring-stiffened (IRS) DT-joints. They concluded that internal rings can significantly increase DT-joint strength after investigating 22 IRS joints. Lan et al. [20] performed numerical parametric studies on stiffener position, depth, and thickness of internal rings on the static strength of IRS DT-joints and concluded that the cause of failure in crown- and saddle-stiffened DT-joints under axial loading of the brace is the development of plastic hinges in the stiffener and chord wall. Masilamani et al. [17] concluded that the internal rings could enhance ultimate strength by 66% based on experimental and numerical investigations of IRS T-joints under axial compression. These studies demonstrate that internal rings, especially in tubular joints, can greatly enhance the ultimate strength of these joints. Their findings suggest significant ultimate strength enhancement, with Lee et al. [19] reporting up to 140% enhancement in the ultimate strength of DT-joints.

The UK Health and Safety Executive commissioned a study [25] to create a databank of in-service ring-stiffened joints. Using in-service data, they determined the uncertainties related to such joints' design (both strength and fatigue). The study has revealed that the approach of elastic closed-ring analysis, which is often employed by operators and consulting engineers, is inadequate for assessing the capacity of ring-stiffened joints in terms of ultimate strength [19]. Azari Dodaran et al. [26] developed parametric equations to determine the static strength of axially loaded tubular KT joints at high temperatures. Sadat Hosseini et al. [27] used fiber-reinforced polymer (FRP) material to reinforce the KT joint to reduce stress concentration factors. They concluded that by including FRP as the strengthening material, a significant reduction of over 50 percent in SCF values was achieved at the saddle location of the central brace, independent of the loading scheme. According to Iqbal et al. [28], the FRP can significantly lower the stress intensity factor of semi-elliptical cracks in KT-joints. Internal ring stiffeners provide the opportunity for further use of FRP during the design stage and during in-service as well. Ahmadi et al. [24, 29–32] conducted comprehensive investigations on KT-joints with internal ring stiffeners, specifically examining stress concentration parameters rather than ultimate strength. The authors [24, 29–32] did not further investigate the ultimate strength, which plays a vital role for the structural integrity and safe operations of offshore structures.

Despite extensive research on the internal ring-reinforced KT-joint, there is a lack of research on three main factors. Firstly, the ultimate strength of stiffened internal rings in KT-joints has not been considered. Secondly, no parametric equations are available to determine the ultimate strength of internal ring-reinforced KT-joints. Thirdly, there is a lack of research on ultimate strength optimization. These are essential design factors to ensure structural integrity, safety, and adherence to industry standards. Well-designed joints transfer the load efficiently, preventing overloading and improving durability and longevity. The pervasive use of these stiffeners in the industry, coupled with the lack of design guidelines in the main offshore codes and standards, emphasizes the need for guidance on strength calculations to assess the structural integrity of platforms with internal ring stiffeners. For ultimate strength, the effects of ring parameters

were studied along with joint parameters, with a novel set of parametric equations proposed. They may be used to calculate the maximum ultimate strength and the strength ratio of an internally reinforced KT joint with high accuracy. The percentage difference between the optimization studies indicated the applicability and high accuracy of the response surface methodology.

2. Research Methodology

The methodology involves parametric modeling in CREO 5.0 software and finite element modeling in ANSYS Workbench 2021, followed by analyzing the response surface design and optimization in Minitab software. The methodology flow chart is shown below in Figure 2. Each step is explained in the following sections:

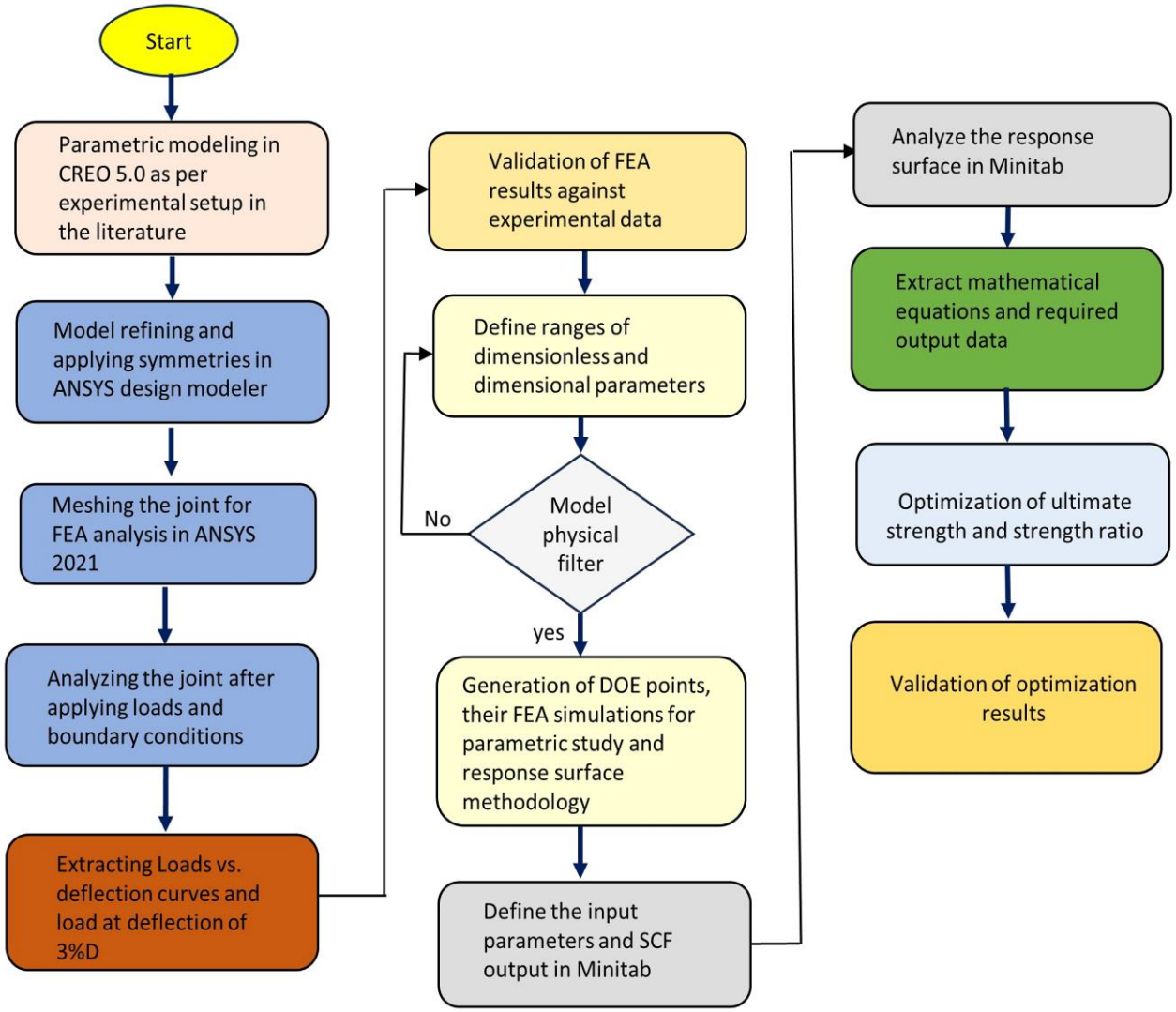

Figure 2. Methodology flowchart

2.1. Finite Element Modeling

Nonlinear structural analysis was performed using ANSYS 2021 software. Material and geometric non-linearities were modeled. The "ARCLEN" method was utilized to address numerical instability. The arc-length method is applicable for solving nonlinear static equilibrium problems that involve instability. The arc-length method is employed to determine the complex orientation in the force-displacement diagrams during the buckling and post-buckling phases. This technique utilizes explicit spherical iterations to preserve orthogonality between perpendicular directions and the arc-length radius [33]. Further explanations about the "ARCLEN" method can be found in the ANSYS Mechanical APDL Theory Reference [33].

Based on the work by Ahmadi & Lotfollahi-Yaghin [24], a KT joint was modeled in Creo 5.0. Three rings were used in the current investigation for each brace, as illustrated in Figure 1 above. Two were joined at crown positions, with the third at the saddle location. Parametric modeling was performed in CREO 5.0 software based on the dimensionless parameters provided in Equations 1 to 9 (Figure 1). The notations and definitions are provided in the "Nomenclature" section.

A sensitivity assessment with different numbers of divisions for all the subparts at the brace chord intersection and coarser mesh for the chord led to the finalization of a mesh of 12419 elements. The parts were modeled in pieces and then assembled, which helped achieve sub-zone meshing, to be described in the next section. Due to the parametric modeling and efficient CREO 5.0 software, the model creation, update, and saving for the next iteration take about 30 seconds. Since the weld had a negligible impact on the strength of the joint, it was excluded from the modeling [19, 17, 20, 34].

Steel was selected for the KT-joint and stiffeners, with a Young's modulus of 207 GPa and a Poisson's ratio of 0.3 [27, 35]. The tangential modulus was taken as 1/100 of Young's modulus [36]. For FEA analysis, the model was imported into the ANSYS 2021 software. Only 1/4 of the complete KT-joint is required to be modeled owing to the XY-plane and YZ-plane symmetries in the joint geometry and loading. Symmetries and model refinement were adopted in the ANSYS design modeler. The parts were modeled in pieces to achieve the best configuration for mesh generation and assembled in CREO 5.0 to achieve the best mesh for the KT-joint analysis, as shown in Figure 3. A sub-zone method was employed for mesh generation in the model to achieve a better result.

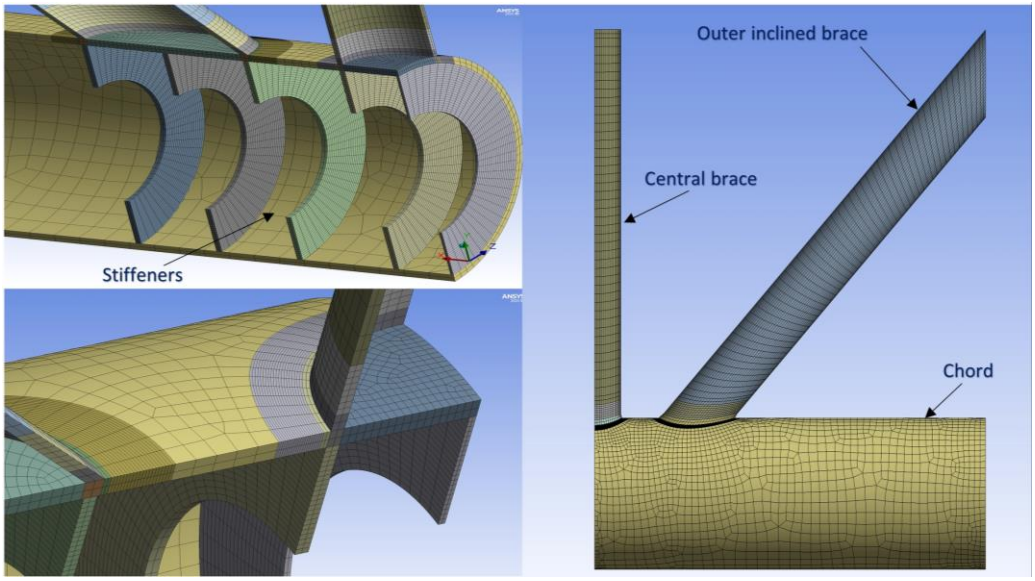

Figure 3. Mesh generated for FEA analysis of KT-joint in ANSYS 2021

A balanced axial load was imposed on the central brace top until the deformation reached 3% of the chord diameter. The highest point on the load-displacement curve often determines the ultimate strength of the joint. The highest point can be achieved if the load-displacement curve has a distinct peak; however, if the load-deflection curves lack a distinct peak, the load at 3% deformation is taken as the ultimate static strength of the KT-joint [37–40].

Figure 4 illustrates the loads and boundary conditions implemented in the experimental investigation by Ahmadi & Lotfollahi-Yaghin [24]. The ends of the outer inclined brace and the chord were fixed.

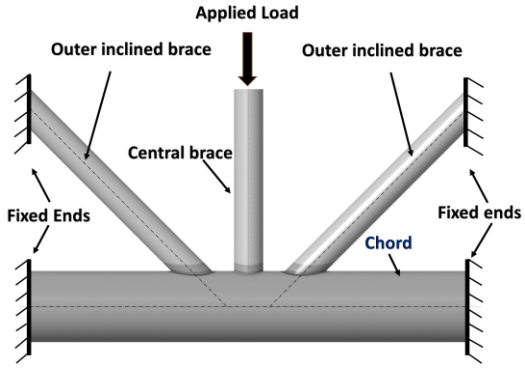

Figure 4. Applied loads and boundary conditions

2.2. Validation of FEA Results against Experimental Data

To the best of the authors' knowledge, no experimental data is available for the ultimate strength of the internal ring-reinforced KT-joint. So, to validate the FE results, the experimental work on the T-joint by Masilamani & Nallayarasu [17], who used the peak load as the ultimate strength of the joint, was considered, where the T-joints were simulated in

ANSYS software and validated against the experimental results. Three T-joint types were modeled and analyzed for the dimensions and material properties used. The first joint was an unstiffened T-joint, the second was a plain ring stiffened joint, and the third was a flanged ring stiffened joint.

Figure 5 illustrates the load-deflection curves of three T-joints extracted from experimental and FEA analyses. A comparison of the FEA results and experimental data [17] is shown in Figure 5, showing a strong correlation between the simulation results and experimental data, proving that numerical models can reliably estimate the ultimate strength of the T joint.

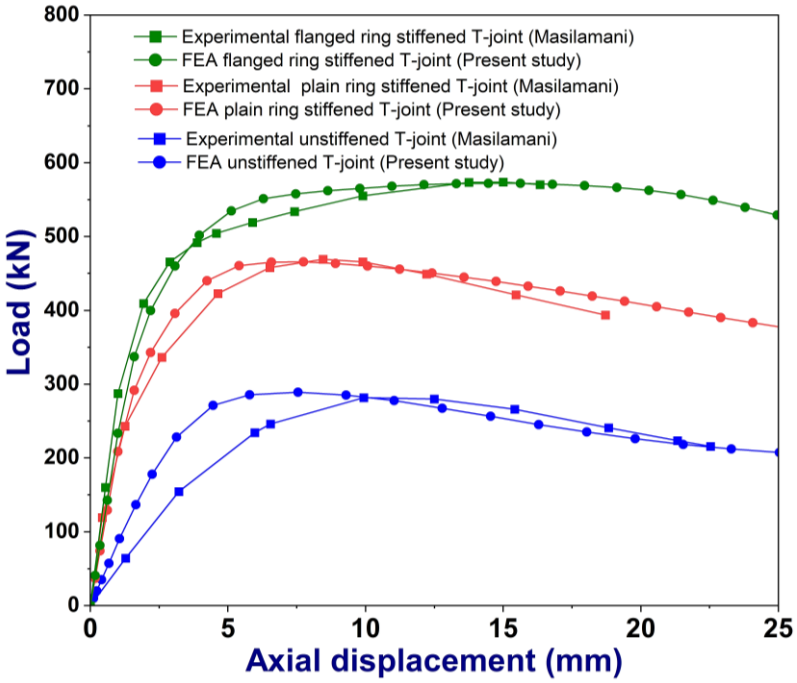

Figure 5. Validation of FEA results against experimental data [17]

Table 1 lists the ultimate strength of the T-joints from experimental and FEA simulations. The percentage error between the experiment and FEA simulations is between 0.2% and 2.3%. The comparison indicates that the FEA model can reliably estimate the ultimate strength of tubular joints.

Table 1. Comparison of FEA results and experimental results [17]

Ultimate strength	Results		
	Experimental	FEA (present study)	% Error
Un-stiffened T-joint	282.26	289.05	2.3 %
Plain ring-stiffened T-joint	468.03	465.56	0.5 %
Flanged ring-stiffened T-joint	573.38	572.20	0.2 %

Figures 6 to 8 show the failed samples of the unstiffened, plain, and flanged ring-stiffened T-joints obtained from both experiments [17] and the numerical simulations. The von Mises stress pattern (Figures 6 to 8-c and 8-d) and equivalent plastic strain pattern (Figures 6 to 8-e) on the deformed shapes (Figures 6, 8-a, and 8-b) of the joints from numerical simulations are derived at the specimen's failure displacements. Figures 6 to 8 display the distorted shapes from the numerical simulation without any magnification factor. These shapes exhibit a high degree of similarity to those observed in the specimen after failure for every joint under investigation. These shapes indicate that all tested joints fail due to localized deformation of the chord wall, which is accompanied by the chord's ovalization [17].

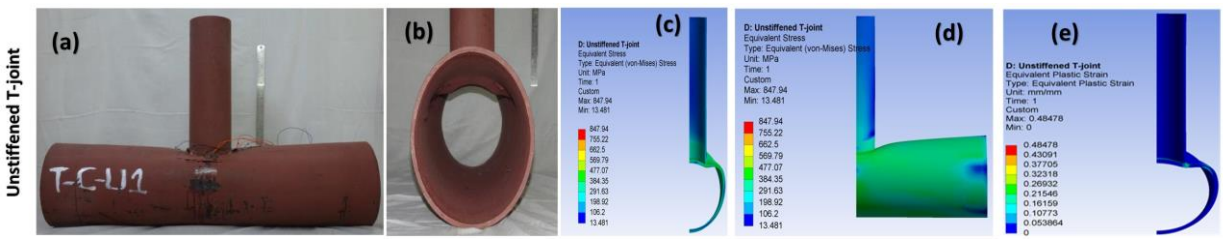

Figure 6. Experimental failed unstiffened T-joint and numerical results [17]

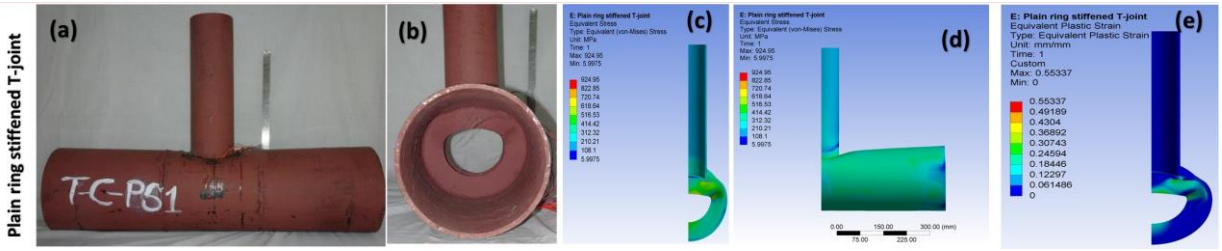

Figure 7. Experimental failed plain ring stiffened T-joint and numerical results [17]

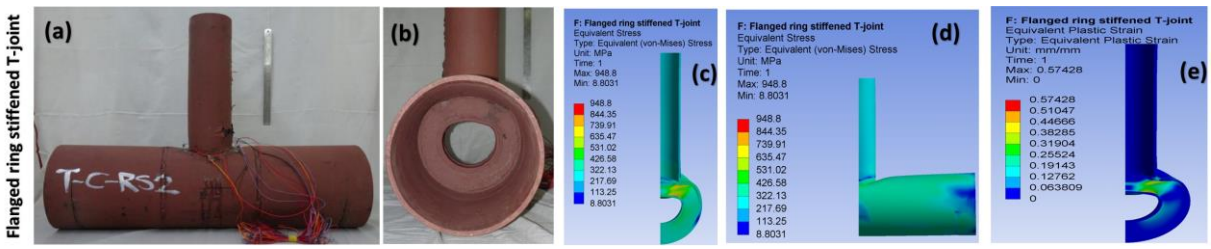

Figure 8. Experimental failed flanged ring stiffened T-joint and numerical results [17]

In an unstiffened joint, the chord undergoes yielding when a load is applied up to its elastic limit. After reaching the ultimate strength, the chord wall buckles and ovalizes due to large displacements. This buckling forces the brace to press the chord, accelerating the ovalization. In contrast, in the plain ring stiffened T-joint and the flanged ring stiffened T-joint, the stiffener reinforces the chord at its ultimate strength, reducing ovalization.

In an unstiffened T-joint, the saddle region experiences higher stresses than the crown region. The stiffener experiences higher stress levels in a plain-ring stiffened T-joint, as depicted in Figures 6–8c. The higher stress in stiffeners suggests that the stiffeners experience a significant amount of stress compared to the chord, with the region between the flange and the chord in a flanged ring-strengthened T-joint subjected to higher stress levels.

The region of maximum strain correlates to the location of maximum stress (Figures 6 to 8-c and 8-e). In an unstiffened T-joint, the critical location is at the intersection of the brace and chord. However, in stiffened joints, the critical location is at the web of the stiffeners (Figures 6 to 8-e).

It is clear from Figure 6-8 (c & d) that the failed specimen of unstiffened, plain ring stiffened, and flanged ring stiffened joints [17] depicted in Figures 6 to 8-b resembles the deformed shape at the location of the brace-chord intersection from the numerical simulation.

2.3. Parametric Study

In this work, the effect of ring parameters and joint parameters on the ultimate strength of KT joints is investigated to develop a new set of equations for determining the ultimate strength and the strength ratio, as well as identifying the internally reinforced KT joint configuration that maximizes both ultimate strength and the strength ratio.

Table 2 lists the dimensional and dimensionless parameters and their corresponding values for the parametric study. They cover the most practical ranges used in the tubular joints of the offshore industry.

Table 2. Parameters and their values

No.	Type of parameter	Parameter	Value	References
1	Dimensionless	β	0.4-0.6	[24, 30–32, 41]
2		γ	16-24	[24, 30–32, 41]
3		τ	0.6-0.9	[24, 30–32, 41]
4		ζ	0.1-0.6	[24, 30–32, 41]
5		λ	0.2-1	[20]
6		δ	0.1-0.2	[17, 19, 25]
7		ψ	0.4-0.8	[19, 25]
8	Dimensional	θ	30˚-60˚	[24, 30–32, 41]

Efthymiou [42] has shown that to guarantee that the stresses at the brace/chord intersection are unaffected by the end condition, a sufficiently long chord larger than six chord diameters (i.e., $\alpha \geq 12$) must be utilized. All the models in the

current investigations were assigned an α value of 12.3, and an αb value of 15 was chosen for all joints, as the stress distribution has a negligible effect due to brace length [37].

As shown in Figure 1, internal rings were positioned relative to the brace diameter at a distance of $\lambda = a.w_s$, where w_s is the distance between the outer stiffener's center in sections A-A along the longitudinal axis of the chord, with "a" varying from 0.2 to 1 [20]. For the central brace, w_s is the same as the diameter of the brace, while it differs in outer inclined braces due to their angle with the chord. Three stiffeners were used under each brace. The central stiffener was always at the saddle location [19], and the outer two stiffeners were placed with reference to λ.

2.4. Generation of Design of Experiments (DoE) Dataset

The geometry of the internally ring-reinforced KT-joint is defined by dimensionless and dimensional parameters (Figure 1). The set of dimensionless and dimensional parameters were selected to build a dataset for the Design of Experiments (DoE) according to the established criteria in the offshore sector (Table 2). A dataset consisting of 420 design points was utilized for simulation. CREO 5.0 was used to do parametric modeling of the IRS KT-joint.

3. Results and Discussion

After simulations, the effect of different joint and ring parameters on the initial stiffness, ultimate strength, and strength ratio was studied. The details of each section are given below. Each combination enhances the ultimate strength of the KT-joint. Overall, the results show that the internal ring stiffened joints can significantly enhance ultimate strength [19].

To evaluate the enhancement in maximum strength resulting from ring parameters, a new parameter Ω is included. The Ω is the ratio of the ultimate strength of the joint with ring stiffeners to the ultimate strength without ring stiffeners.

In all cases, both the ring stiffened joints and unstiffened joints achieve ultimate strength at the same deformation levels. This suggests that the inner rings do not impact the ductility of the tubular joints. A similar pattern was noted in the study conducted by Masilamani et al. [17]. The inner ring and cylinder-formed T-section have greater bending stiffness than the cylindrical section, the ring-stiffened joint can withstand more bending stress, increasing the KT-joint's ultimate strength.

The strength of the ring was shown to be significantly influenced by the thickness (t_s) and height (h_s) of the ring, as shown in Figure 1. The thickness and width of rings exhibit a direct relationship with the bending stiffness [19], hence enhancing the ultimate strength of the KT-joint. Increasing the parameter γ results in a decrease in the thickness of the KT-joint. While the parameter γ does not affect the load deflection curves, it does decrease the ultimate strength of the tubular KT-joint. In all simulations, the failure mechanism of the KT-joint was the development of plastic hinges and the yielding of the chord wall. The same observation was made by Xiaoyi et al. [20]. The spacing λ parameter exhibits both increasing and decreasing behaviour for ultimate strength [20].

3.1. Effect of β on the Initial Stiffness, Ultimate Strength, and Strength Ratio

The parameter β represents the brace-to-chord diameter ratio; an increase in β at constant chord diameter increases the brace diameter. The influence of β on the initial stiffness, ultimate strength, and strength ratio of KT-joint and the interaction between β and ring parameters (λ, δ, and ψ) are investigated. A series of simulations were conducted to examine the impact of β and its interactions with ring parameters (λ, δ, and ψ). In the interest of brevity, this section includes six graphs, as shown in Figures 9-a to 9-f, although several comparison graphs were used to analyze the impact. The load-deflection curves for the simulation models are shown in Figures 9-a, 9-c and 9-e. Figures 9-b, 9-d and 9-f. illustrates the ratio between the ultimate strength of the stiffened joint and the unstiffened joint for the same models. There are three different values of β in the six charts: 0.4, 0.5, and 0.6. The values of the remaining joint parameters, namely γ, τ, θ, and ζ, are constant throughout all of these simulations, with γ = 16.25, τ = 0.6, θ = 45°, and ζ = 0.3. On the other hand, the ring parameters, λ, δ, and ψ, have different values in each scenario. δ has values of 0.1 and 0.2, λ has values of 0.2, 0.6 and 1, and ψ has values of 0.4, 0.6, and 0.8.

The graphs show that increasing the β leads to higher ultimate strength and initial stiffness but a lower strength ratio [1, 18]. By increasing β from 0.4 to 0.5, the initial stiffness increases between 4% and 7%, the ultimate strength increases between 2% and 15%, but the strength ratio decreases between 6% and 16%. By increasing β from 0.4 to 0.6, the initial stiffness increases between 10% and 16%, the ultimate strength increases between 3% and 24%, but the strength ratio decreases between 15% and 29%. The strength ratio indicates that the effect of ring parameters is more significant when β is small. The effect is more significant due to the increasing ultimate strength of unstiffened joints with higher β values [19]. These trends suggest that the internal rings were more efficient in enhancing the ultimate strength for joints with small β, but had a limited impact on joints with large β [1].

For constant values of β, when increasing the spacing λ from 0.2 to 0.1, the initial stiffness increases up to 3%, and the ultimate strength and the strength ratio increase up to 10%. For all values of β when δ=0.1, the ultimate strength and

the strength ratio decrease by up to 5% when spacing increases from 0.6 to 1.

By increasing δ from 0.1 to 0.2, the initial stiffness increases between 6% and 16%, and the ultimate strength and the strength ratio increases between 2% and 28%. By increasing ψ from 0.4 to 0.8, the initial stiffness increases up to 9%, and the ultimate strength and the strength ratio increase between 1% and 19%.

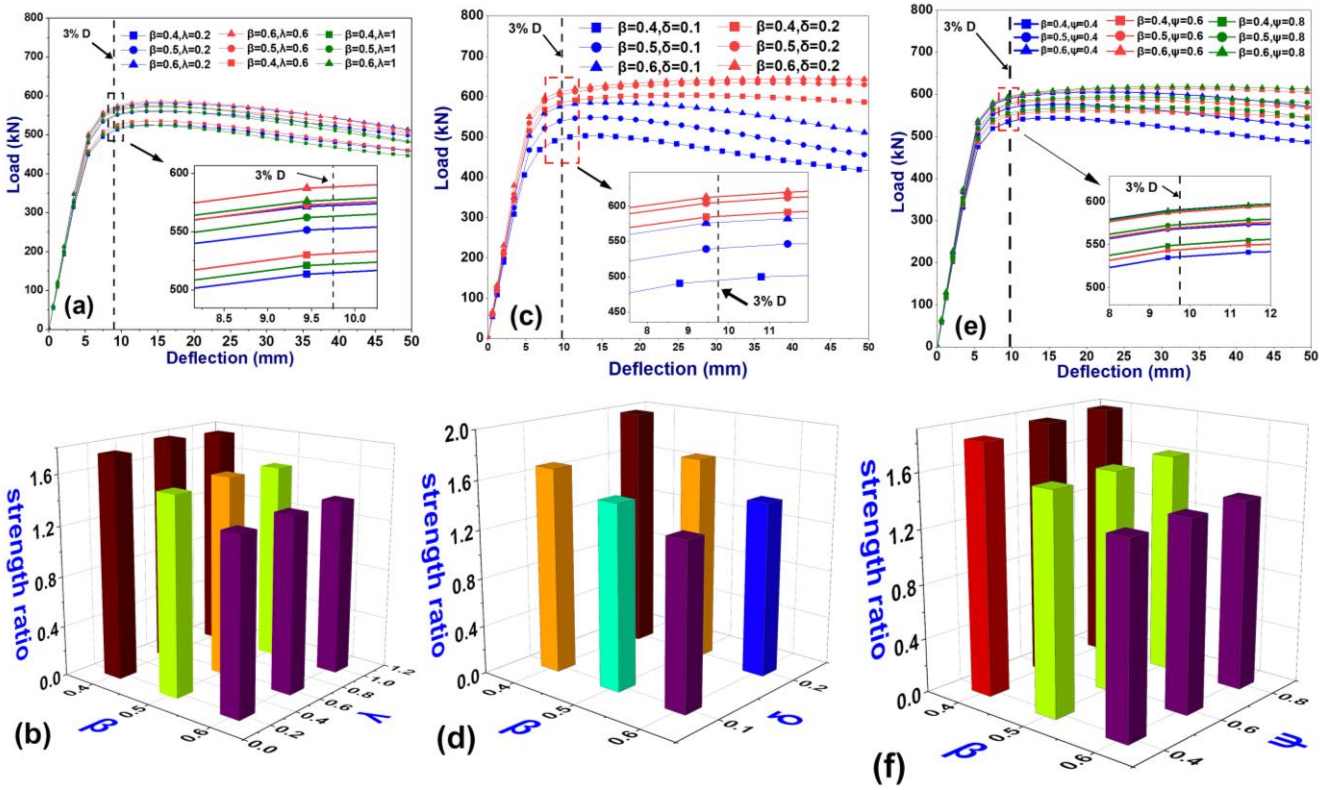

Figure 9. Effect of β on the initial stiffness, ultimate strength, and the strength ratio, where γ=16.25, τ=0.6, θ=45°, ζ=0.3, and for (a) and (b) δ=0.1, ψ=0.8, and for (c) and (d) λ=0.6, ψ=0.6, and for (e) and (f) λ=0.2 δ=0.2

3.2. Effect of γ on the Initial Stiffness, Ultimate Strength, and Strength Ratio

The ratio of chord diameter to twice the thickness of the chord is represented by the parameter γ, with an increase in γ at constant chord diameter resulting in a decrease of chord thickness. The influence of γ on the initial stiffness, ultimate strength, and strength ratio of the KT-joint; and the interaction between γ and ring parameters (λ, δ, and ψ) are investigated. A series of simulations were conducted to examine the impact of γ and its interactions with ring parameters (λ, δ, and ψ). In the interest of brevity, this section includes just six graphs from Figures 10-a to 10-f, although several comparison graphs were used to analyze the impact. The load-deflection graphs for the simulation models are shown in Figures 10-a, 10-c, and 10-e. Figures 10-b, 10-d, and 10-f illustrates the ratio between the ultimate strength of the stiffened joint and the unstiffened joint for the same models. In each of the six charts, there are three distinct values of γ, which are 16.25, 20, and 24. The values of the remaining joint parameters, namely β, τ, θ, and ζ, are constant throughout all of these simulations, with β = 0.4, τ = 0.6, θ = 45°, and ζ = 0.3. On the other hand, the values of the ring parameters, namely λ, δ, and ψ, differ across the cases. δ has values of 0.1 and 0.2, λ has values of 0.2, 0.6, and 1, and ψ has values of 0.4, 0.6, and 0.8.

The graphs show that decreasing the γ leads to higher ultimate strength and initial stiffness but a lower strength ratio [18]. By decreasing γ from 24 to 20, the initial stiffness increases between 18% and 61%, the ultimate strength increases between 21% and 29%, but the strength ratio decreases between 6% and 12%. By further decreasing γ from 20 to 16.25, the initial stiffness increases between 44% and 124%, the ultimate strength increases between 49% and 71%, but the strength ratio decreases between 11% and 23%. The strength ratio indicates that when γ is large, strength enhancement due to ring parameters is more significant. The effect is more significant due to the increasing ultimate strength of unstiffened joints with smaller γ values [1].

For constant values of γ, increasing the spacing λ from 0.2 to 1, the initial stiffness increases up to 3%, and the ultimate strength and the strength ratio increase up to 16%. For all values of γ when δ=0.1, the ultimate strength and the strength ratio decrease by up to 5% when spacing λ increases from 0.6 to 1. By increasing δ from 0.1 to 0.2, the initial stiffness increases between 8% and 22%, and the ultimate strength and the strength ratio increases between 8% and 34%. By increasing ψ from 0.4 to 0.8, the initial stiffness increases between 3% and 13%, and the ultimate strength and the strength ratio increases between 4% and 28%.

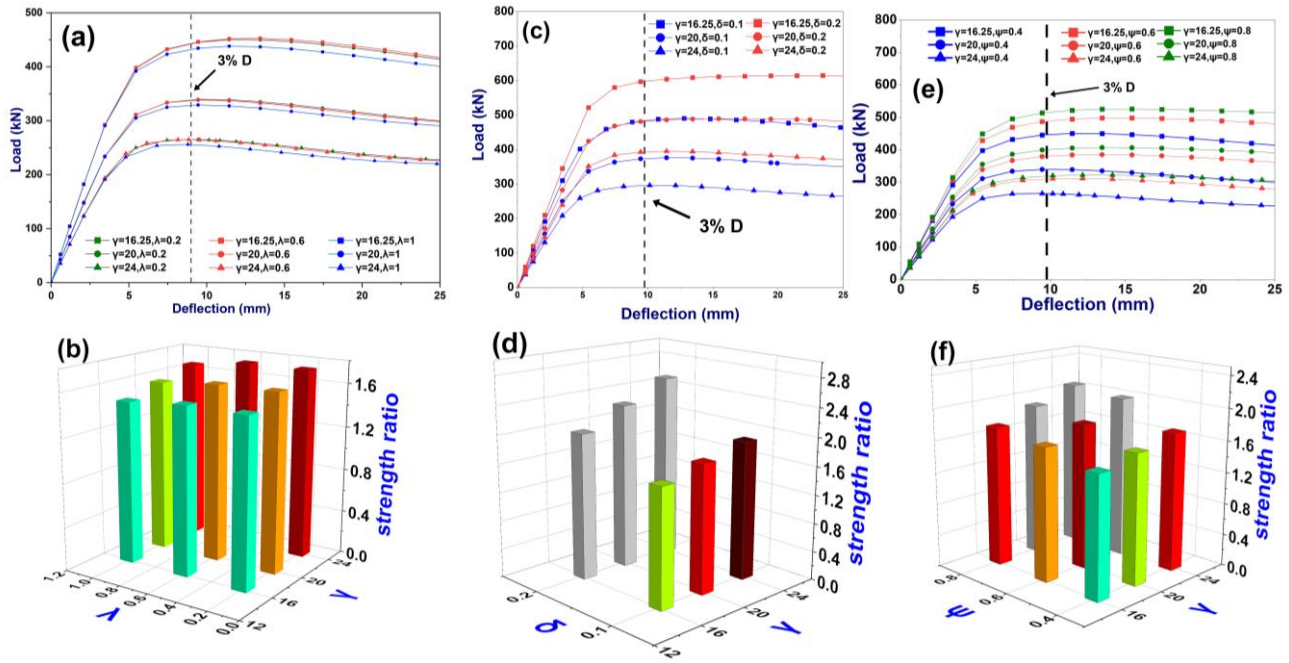

Figure 10. : Effect of γ on the initial stiffness, ultimate strength, and the strength ratio, where β =0.4, τ=0.6, θ=45̊, ζ=0.3 for (a) and (b) δ=0.1, ψ=0.4, for (c) and (d) λ=1, ψ=0.6 and for (e) and (f) λ=0.2, δ=0.1

3.3. Effect of τ on the Initial Stiffness, Ultimate Strength, and the Strength Ratio

The brace to chord thickness ratio is represented by the parameter τ; an increase in τ at constant chord thickness increases the brace thickness. The influence of τ on the initial stiffness, ultimate strength, and strength ratio of the KT-joint and the interaction between τ and ring parameters (λ, δ, and ψ) are investigated. A series of simulations were conducted to investigate the impact of τ and its interactions with ring parameters (λ, δ, and ψ). In the interest of brevity, this section includes just six graphs from Figures 11-a to 11-f, although several comparison graphs were used to analyze the impact. Load deflection curves for the simulation models are shown in Figures 11-a, 11-c and 11-e. Figures 11-b, 11-d and 11-f illustrates the ratio between the ultimate strength of the stiffened joint and the unstiffened joint for the same models. In each of the six charts, there are two distinct values of τ, which are 0.6 and 0.9. The values of the remaining joint parameters, namely β, γ, θ, and ζ, are constant throughout all of these simulations, with β = 0.4, γ = 16.25, θ = 45̊, and ζ = 0.3. On the other hand, the values of the ring parameters, namely λ, δ, and ψ, differ. δ has values of 0.1 and 0.2, λ has values of 0.2, 0.6, and 1, and ψ has values of 0.4, 0.6, and 0.8.

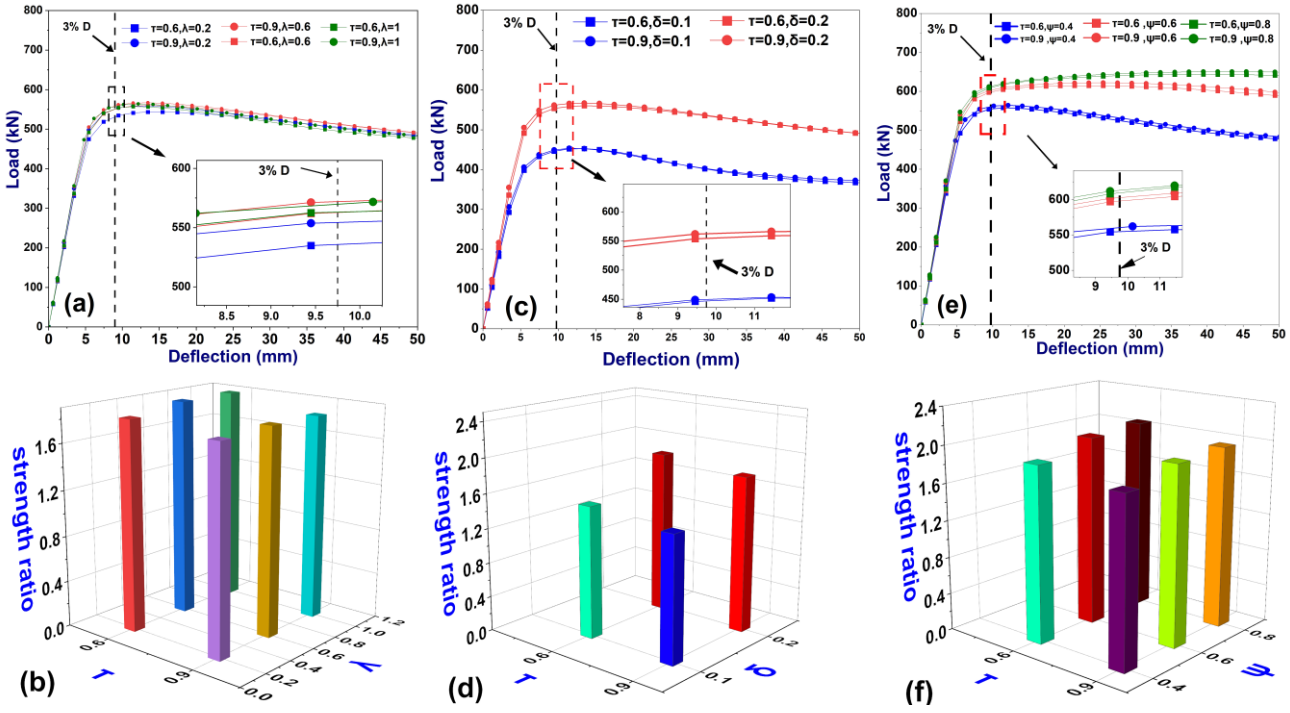

Figure 11. Effect of τ on the initial stiffness, ultimate strength, and the strength ratio, where β =0.4, γ=16.25, θ=45̊, ζ=0.3 for (a) and (b) δ=0.2, ψ=0.4, for (c) and (d) λ=0.6, ψ=0.4 and for (e) and (f) λ=1, δ=0.2

The comparison graphs show that increasing the τ decreases the strength ratio but increases the initial stiffness and ultimate strength. By increasing τ from 0.6 to 0.9, the strength ratio decreases between 2% and 5%, but the initial stiffness increases between 4% and 7%, and the ultimate strength increases between 1% and 5%.

For constant values of τ, increasing the spacing λ from 0.2 to 1, the initial stiffness increases up to 2%, and the ultimate strength and the strength ratio increase up to 10%. For all values of τ when δ=0.1, the ultimate strength and the strength ratio decrease by up to 3% when spacing increases from 0.6 to 1. By increasing δ from 0.1 to 0.2, the initial stiffness increases between 8% and 18%, and the ultimate strength and the strength ratio increase between 8% and 28%. By increasing ψ from 0.4 to 0.8, the initial stiffness increases between 3% and 10%, and the ultimate strength and the strength ratio increases between 4% and 20%.

3.4. Effect of θ on the Initial Stiffness, Ultimate Strength, and the Strength Ratio

As shown in Figure 1, the θ angle is the angle between the main chord and the outer inclined braces. The influence of θ on the strength ratio, ultimate strength, and the initial stiffness of the KT-joint and the interaction between θ and ring parameters (λ, δ, and ψ) are investigated. A series of simulations were conducted to investigate the impact of θ and its interactions with ring parameters (λ, δ, and ψ). In the interest of brevity, this section includes just six graphs from Figures 12-a to 12-f, although several comparison graphs were used to analyze the impact. The load-deflection graphs for simulation models are shown in Figures12-a, 12-c and 12-e. Figure 12-b, 12-d and 12-f illustrates the ratio between the ultimate strength of the stiffened joint and the unstiffened joint for the same models. In each of the six charts, there are three distinct values of θ, which are 30̊, 45̊ and 60̊. The values of the remaining joint parameters, namely β, γ, τ, and ζ, are constant throughout all of these simulations, with β = 0.4, γ = 16.25, τ = 0.6, and ζ = 0.3. On the other hand, the values of the ring parameters, namely λ, δ, and ψ, differ across the cases. δ has values of 0.1 and 0.2, λ has values of 0.2, 0.6, and 1, and ψ has values of 0.4, 0.6, and 0.8.

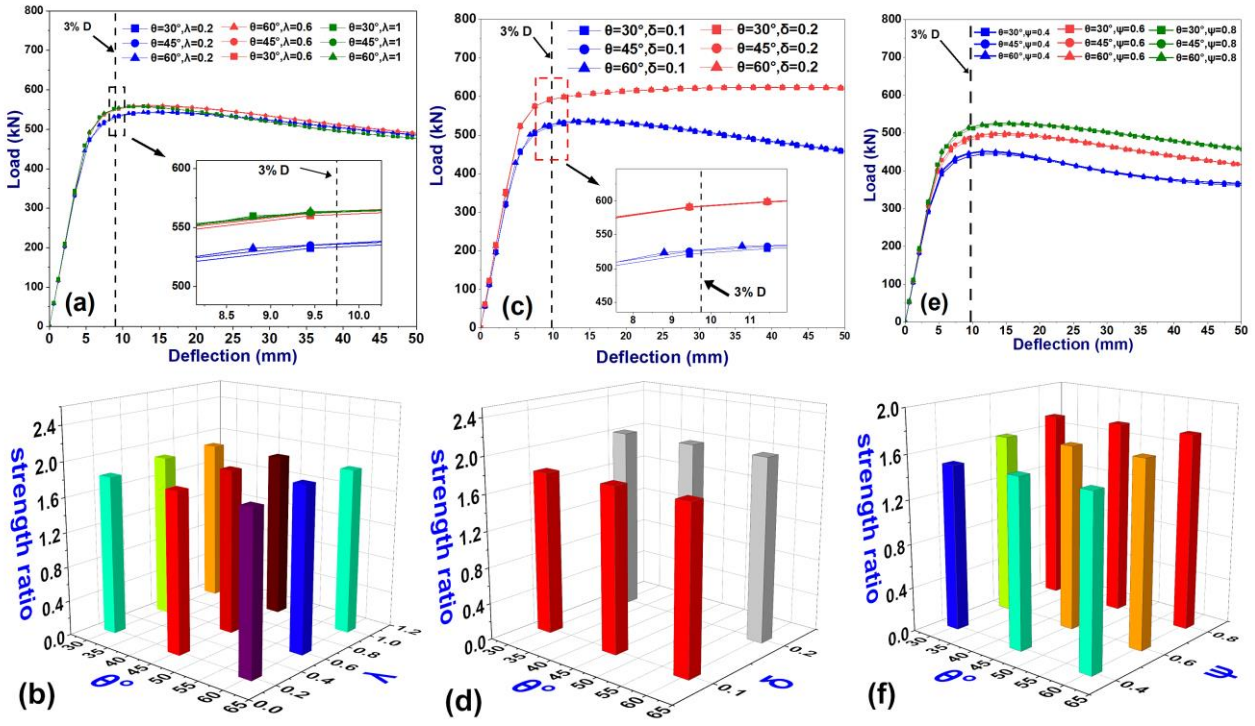

Figure 12. Effect of θ on the initial stiffness, ultimate strength, and the strength ratio, where β =0.4, γ=16.25, τ=0.6, ζ=0.3 for (a) and (b) δ=0.2, ψ=0.4, for (c) and (d) λ=0.2, ψ=0.4 and for (e) and (f) λ=1, δ=0.2

The comparison graphs show that the angle θ does not have much impact on the strength ratio, ultimate strength, and initial stiffness. By increasing the angle θ from 30̊ to 60̊, the difference between strength ratio, ultimate strength, and the initial stiffness is less than 2%, which makes this parameter θ insignificant.

When θ is constant, the initial stiffness, ultimate strength, and strength ratio follow the same ranges due to ring parameters as in constant τ values discussed in the previous section 4.3.

3.5. Effect of ζ on the Initial Stiffness, Ultimate Strength, and Strength Ratio

As shown in Figure 1, the parameter ζ is the distance between the central and the outer inclined brace. The influence of ζ on the initial stiffness, ultimate strength, and strength ratio of the KT-joint and the interaction between ζ and ring

parameters (λ, δ, and ψ) are investigated. A series of simulations were conducted to investigate the impact of ζ and its interactions with ring parameters (λ, δ, and ψ). In the interest of brevity, this section includes just six graphs from Figures 13-a to 13-f, although several comparison graphs were used to analyze the impact. The load-deflection graphs for simulation models are shown in Figures 13-a, 13-c, and 13-e. Figures 13-b, 13-d, and 13-f illustrates the ratio between the ultimate strength of the stiffened joint and the unstiffened joint for the same models. There are three different values of ζ in all of the six charts: 0.1, 0.3, and 0.6. The values of the remaining joint parameters, namely γ, τ, θ, and β, are consistent throughout all of these simulations, with γ = 16.25, τ = 0.6, θ = 45°, and β = 0.4. On the other hand, the ring parameters, λ, δ, and ψ, have different values in each scenario. δ has values of 0.1 and 0.2, λ has values of 0.2, 0.6 and 1, and ψ has values of 0.4, 0.6, and 0.8.

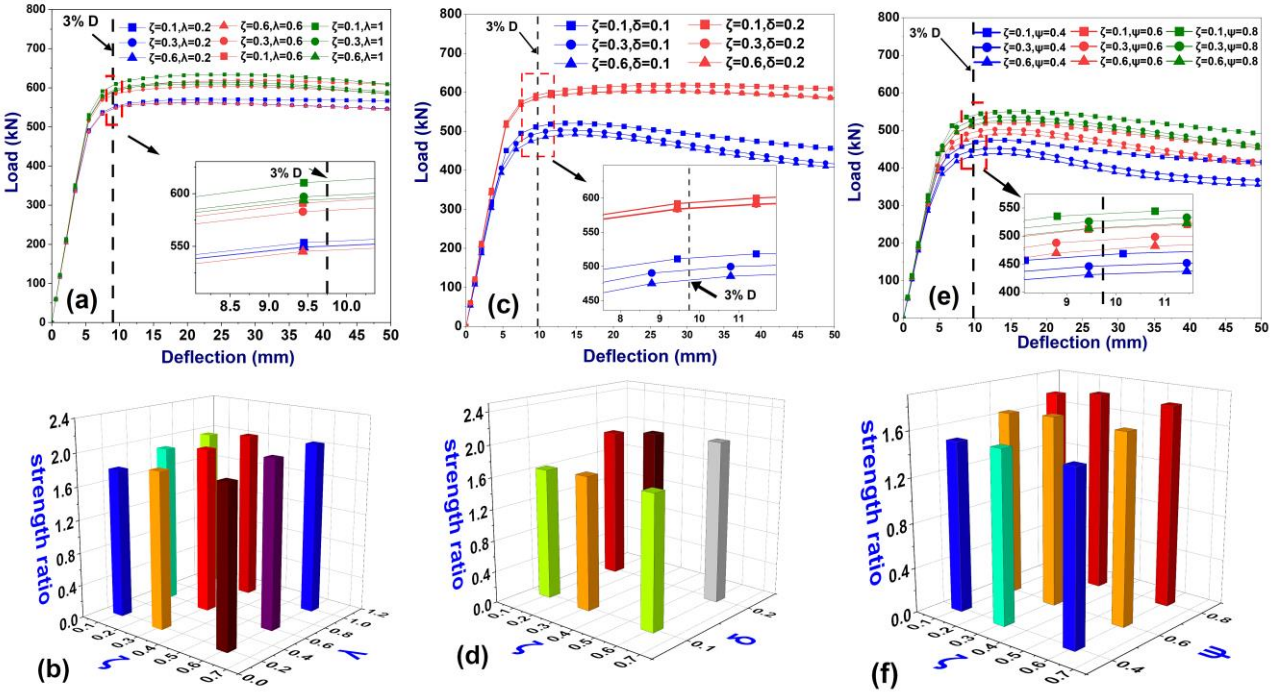

Figure 13. Effect of ζ on the initial stiffness, ultimate strength, and the strength ratio, where β =0.4, γ=16.25, τ=0.6, θ=45° for (a) and (b) δ=0.2, ψ=0.6, for (c) and (d) λ=0.6, ψ=0.6 and for (e) and (f) λ=0.6, δ=0.1

The comparison graphs show that decreasing the value of ζ increases the ultimate strength and initial stiffness. However, the strength ratio exhibits both increasing and decreasing behaviors. When ζ is reduced from 0.6 to 0.1, the ultimate strength and initial stiffness both increase 9% and 8%, respectively. However, the change in strength ratio ranges from -6% to 2%, indicating both an increase and a decrease.

For constant values of ζ, increasing the spacing λ from 0.2 to 1, the initial stiffness increases up to 3%, and the ultimate strength and the strength ratio increase up to 12%. For all values of ζ when δ=0.1, the ultimate strength and the strength ratio decrease by up to 3% when spacing increases from 0.6 to 1. By increasing δ from 0.1 to 0.2, the initial stiffness increases between 7% and 19%, and the ultimate strength and the strength ratio increase between 6% and 30%. By increasing ψ from 0.4 to 0.8, the initial stiffness increases up to 10%, the ultimate strength and the strength ratio increase between 3% and 20%.

4. Response Surface Methodology

RSM has been shown to produce precise and comprehensive predictions [43], their use in mathematical modeling of ultimate strength and strength ratio of internally ring reinforced KT-joints is considered here. Seven dimensionless parameters and one-dimensional parameter, as listed in Table 2, were used as input components in the response surface technique. A total of 420 FEA models were developed utilizing optimal design techniques. Optimal design is a superior alternative in cases where the central composite and box-Behnken designs do not meet the specified requirements. Evaluation of parameters within the context of an optimal design is characterized by minimal variation and no bias. The equation represented by Equation 10 is a quadratic model that is an ideal predictor. It can be employed to forecast the conditions under which reactions of significance may occur [43]:

$$y = \beta_0 + \sum_{i=1}^{k} \beta_i x_i + \sum_{i=1}^{k} \beta_{ii} x_i^2 + \sum_{j=2}^{k} \cdot \sum_{i=1}^{j=1} \beta_{ij} x_i x_j + \in \quad (10)$$

A predictive model for the ultimate strength and the strength ratio is given by Equation 10. The constant value "β◦" is indicated in this context. "βii" designates quadratic regression, but "βi" denotes linear regression. Furthermore, the

relationship between the variables "xi" and "xj" is specified by "βij." The random error component is represented by the symbol "∈". As indicated in Table 2, the variables β, γ, θ, ζ, λ, and ψ each have three levels, while τ and δ have two levels. To investigate the impact of a joint parameter, such as β, from the set of joint parameters (β, ζ, τ, θ, γ) and its interaction with ring parameters (λ, δ, ψ), all other joint parameters γ, τ, θ, ζ (except β) were held constant. Subsequently, all possible combinations of the joint parameter β with the ring parameters (λ, δ, ψ) were examined using the ANSYS software. Then, for combinations of γ, other joint parameters (β, τ, θ, ζ) were given a constant value. Subsequently, all possible combinations of the joint parameter γ with the ring parameters (λ, δ, ψ) were determined using the ANSYS software in the same way combinations of (τ, θ, ζ) were determined in ANSYS [5, 44].

4.1. The Analysis of Variance (ANOVA) for Response Surface Models

The design utilized the response surface derived from Equation 10 for the two considered responses (ultimate strength and the strength ratio). The quadratic model was the most suitable fit for the required outputs (ultimate strength and the strength ratio). The response surface was modeled using a complete quadratic model, resulting in 35 terms for each equation.

The ANOVA model was validated with a 95% confidence interval at a significance level of 5% [45]. The outcome of the ANOVA analysis is presented in Appendix I. The model reduction process was conducted using Minitab software, wherein only the terms with P values less than 0.05 were retained, while those with larger P values were excluded. Table 3 shows the validation parameters corresponding to each model. The output equations obtained by applying response surface methods to predict the model are shown below.

Table 3. Model validation

Model validation parameters	Responses	
	Ultimate strength	Strength ratio
S $\times 10^{-2}$	6.587	6.808
R-sq (R^2)	97.51%	97.47%
R-sq(adj)	97.23%	97.20%
R-sq(pred)	96.89%	96.86%

4.2. Output Equations for Ultimate Strength and Strength Ratio

Ultimate strength = 559.2 + 1392 β - 70.33 γ + 33.9 τ + 0.1305 θ - 169.9 ζ + 20.8 λ + 2221.3 δ + 637.5 ψ - 450 β*β + 1.2078 γ*γ + 90.7 ζ*ζ- 52.82 λ * λ - 215.6 ψ * ψ - 53.6 β* λ - 2424 β* δ - 398.7 β* ψ - 22.29 γ* δ - 44.2 τ* λ + 168.8 τ* δ - 24.99 ζ* λ + 370.6 ζ* δ + 34.0 ζ* ψ + 501.4 λ * δ + 77.75 λ * ψ - 882.2 δ * ψ (11)

Strength ratio = 0.748 + 0.682 β - 0.01754 γ - 0.1546 τ + 0.000528 θ + 0.1588 ζ- 0.0393 λ + 3.942 δ + 1.608 ψ - 0.4291 ζ*ζ - 0.2052 λ * λ - 0.8312 ψ * ψ - 0.2667 β* λ - 10.525 β* δ - 1.744 β* ψ + 0.00679 γ* λ + 0.2140 γ* δ + 0.05320 γ* ψ - 0.1596 τ* λ + 1.645 ζ* δ + 1.871 λ * δ + 0.2976 λ * ψ - 3.125 δ * ψ (12)

The coefficient of determination (R^2) assesses the accuracy of the model's predictions and is the degree to which the provided data and model align. The variable R^2 is quantified on a scale from 0 to 100 percent. The values of R^2 in the generated model are presented in Table 3, which are 97.51% for ultimate strength and 97.47% for the strength ratio. High R^2 values serve as a reliable indication of the robustness of the built model.

The standard error of the estimate, symbolized as S, quantifies the extent of fluctuation between the predicted and actual values. A decreased S value indicates a heightened coherence between the predicted results and the empirical data. The values of S in the constructed model are provided in Table 3, which are 0.06587 for ultimate strength and 0.06808 for the strength ratio. A greater value of the adjusted R-squared (R-sq(adj)) indicates a more optimal balance between the model's fit quality and its simplicity, which is essential for assuring reliable predictions within the optimization framework. The adjusted R-squared values for the derived model are presented in Table 3, which are 97.23% for ultimate strength and 97.20% for the strength ratio. The assessment of R-squared prediction (R-sq(pred)) is significant in response surface methodology. It serves as an indicator for evaluating the model's ability to anticipate new and unseen data points effectively. A higher value of R-squared (pred) indicates better prediction accuracy, therefore validating the reliability of the response surface model beyond the available data used for model estimation. The values of R-squared (pred) in this established model are presented in Table 3, which are 96.89% for ultimate strength and 96.86% for the strength ratio.

Model accuracy is commonly evaluated using two essential diagnostic tools: actual vs. predicted plots and residual plots. Two distinct types of plots may be observed in the response models depicted in Figures 14 and 15, respectively. For a model to be deemed a satisfactory fit, the data points in a plot illustrating the ultimate strength and the strength ratio extracted from FEA and predicted by the proposed equations should be aligned as closely as possible with the corresponding fitted line. The data points in this specific model instance are diagonally aligned with the fitted line, indicating a strong correlation between the projected values and the strength ratio and ultimate strength derived from FEA. This indicator is a reliable measure of the accuracy of the response models.

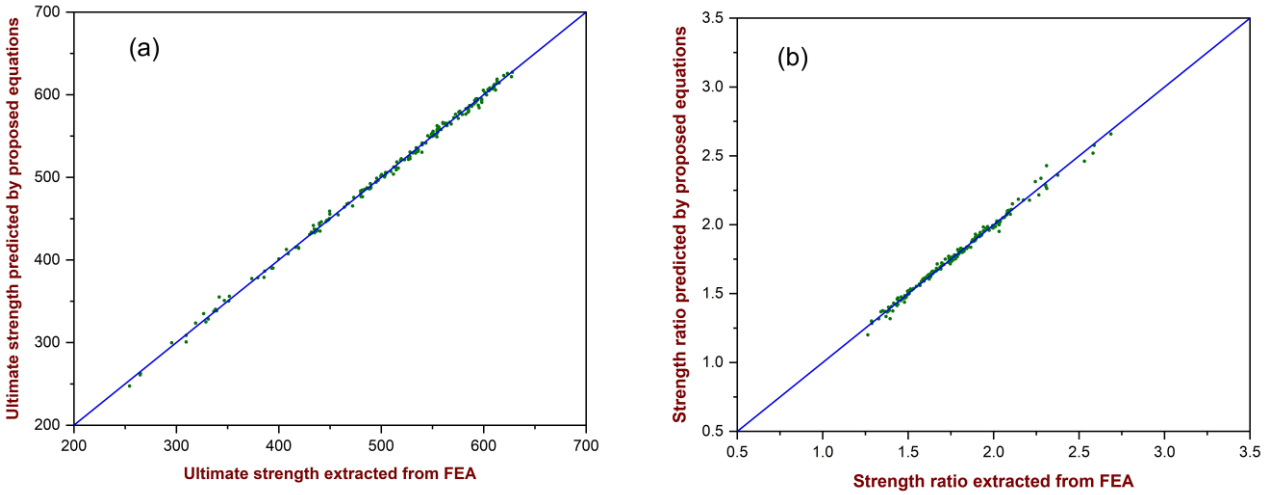

Figure 14. Comparison of ultimate strength and the strength ratio extracted from FEA and predicted by proposed Equations

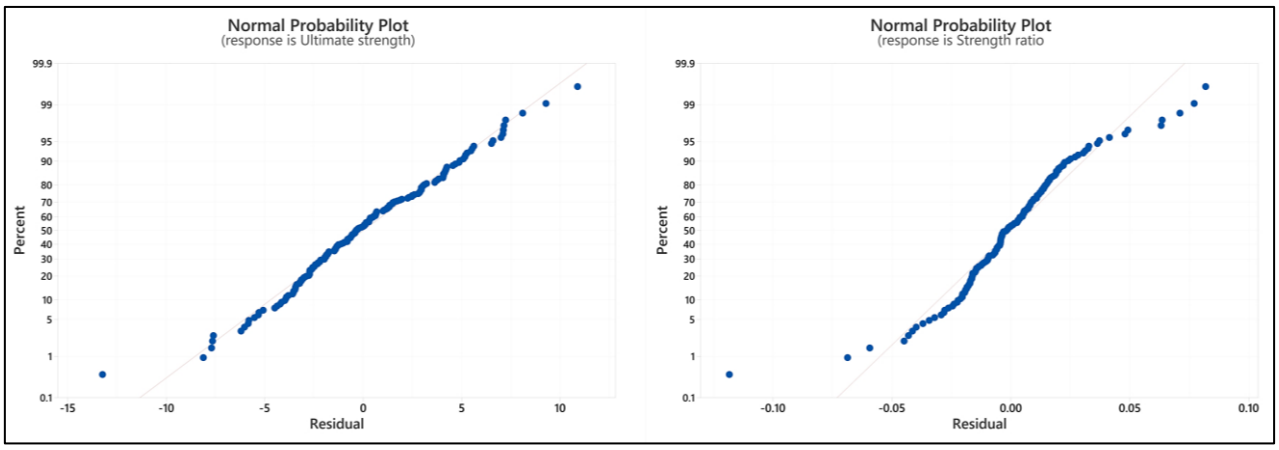

Figure 15. Normal probability plots for ultimate strength and the strength ratio

Figure 15 offers a graphical depiction of residuals' normal plots. This observation supports the notion that error components exhibit uniform distribution, as it illustrates the linearity of the points along the diagonal. A key attribute distinguishing a dependable model is its defining trait. This phenomenon can be attributed to the observation that if the residuals conform to a normal distribution, approximately 95% of them are expected to lie within the range of -2 to +2 to satisfy the criteria for a normal distribution [43]. This analysis shows that all residual plots exhibit conformity, indicating the models' predictive accuracy (see Figure 15).

4.3. Optimization of Ultimate Strength and the Strength Ratio

Optimization was performed in Minitab software to achieve the optimal parameters for maximum ultimate strength and maximum strength ratio. The independent variable of the model underwent optimization to enhance its effectiveness. The optimization process outcome for each answer is ultimately determined by the desirability value, represented by the interval $0 \leq dj \leq 1$. The value in question exhibits a range between 0 and 1. By increasing the value of the dj variable, the resulting outcome can be more advantageous, expressed as a percentage. In the present study, a limit of desirability was established within the range of 0 to 1. When the desirability value reaches 1, it indicates a more positive outcome for the model and increases the reliability of the optimized results in estimating the dependent variable. Optimization of

ultimate strength and the strength ratio concluded that the KT-joint with parameters λ=0.9111, δ=0.2, ψ=0.7030, ζ=0.3, θ=45°, τ=0.90, γ=16.25, and β=0.6 had maximum ultimate strength and the KT-joint with parameters: λ=1, δ=0.2, ψ=0.8, ζ=0.5697, θ=45°, τ=0.61, γ=24, and β=0.41 had maximum strength ratio. The model's desirability for the ultimate strength and the strength ratio are 1 and 0.978, respectively, which indicates that the optimization strategy produced highly desirable outcomes.

$$\text{Error (\%)} = \left(\frac{(Predicted\ value - FEA\ value)}{FEA\ value}\right) \times 100 \quad (13)$$

As shown in Table 4, an FEA verification was performed to determine the discrepancy between the obtained numerical values and the predicted response values resulting from the optimization technique. The model was developed based on the ideal parameters suggested by optimization. The percentage error is calculated to compare predicted values from optimization and FE values with optimized parameters. The data clearly shows that the percentage error for all responses is less than 1.7%. The close correlation between the optimized outcomes and the findings obtained from finite element analysis demonstrates significant accuracy.

Table 4. Results of numerical validation of the optimized value

Response	Predicted	FEA	Error (%)
Ultimate strength	636.31	625.67	1.70
Strength ratio	2.66	2.64	0.76

5. Conclusions

Based on current investigations, the following points were observed.

a) The outcome of the parametric study is summarized below.

- Increasing β leads to higher ultimate strength and initial stiffness but a lower strength ratio. By increasing β from 0.4 to 0.6, the initial stiffness increases between 10% and 16%, the ultimate strength increases between 3% and 24%, but the strength ratio decreases between 15% and 29%. The strength ratio indicates that the effect of ring parameters is more significant when β is small.
- Decreasing the γ leads to higher ultimate strength and initial stiffness but a lower strength ratio. By decreasing γ from 24 to 16.25, the initial stiffness increases between 44% and 124%, the ultimate strength increases between 49% and 71%, but the strength ratio decreases between 11% and 23%. The strength ratio indicates that when γ is large, strength enhancement due to ring parameters is more significant.
- Increasing the τ decreases the strength ratio but increases the initial stiffness and ultimate strength. By increasing τ from 0.6 to 0.9, the strength ratio decreases between 2% and 5%, but the initial stiffness increases between 4% and 7%, and the ultimate strength increases between 1% and 5%.
- By increasing the angle θ from 30° to 60°, the difference between initial stiffness, ultimate strength, and strength ratio is less than 2%, which makes this parameter θ insignificant.
- By decreasing the value of ζ, the initial stiffness and ultimate strength are increased. However, the strength ratio exhibits both increasing and decreasing behaviors. When ζ is reduced from 0.6 to 0.1, the initial stiffness and ultimate strength both increase 8% and 9%, respectively. However, the change in strength ratio ranges from -6% to 2%, indicating both an increase and a decrease.
- The maximum increase in the values of initial stiffness, the ultimate strength, and the strength ratio due to ring parameters (λ, δ, and ψ) are achieved for the constant values of γ.
- The depth parameter (δ) and thickness parameter (ψ) of the rings have a direct relationship with strength ratio, ultimate strength, and the initial stiffness [19]. Increasing depth parameter (δ) from 0.1 to 0.2 increases the initial stiffness between 6% and 22%, and the ultimate strength and the strength ratio increases between 2% and 34%. By increasing the thickness parameter (ψ) from 0.4 to 0.8, the initial stiffness increases up to 9%, and the ultimate strength and the strength ratio increase between 1% and 17%.
- By increasing the spacing parameter (λ) from 0.2 to 0.6, the initial stiffness increases up to 2%, and the ultimate strength and the strength ratio increase up to 12%. By further increasing the spacing parameter (λ) from 0.6 to 0.1, the initial stiffness decreases up to 1%, and the ultimate strength and the strength ratio decrease up to 8% [20].
- With these parameters, as listed in Table 2, the increase in the ultimate strength is at least 30% and up to 170%.

b) The response surface methodology for internally reinforced KT-joint ultimate strength and the strength ratio optimization under compressive load were presented in this study. The response surface model and suggested mathematical formulas provide high precision in predicting the ultimate strength and the strength ratio variables. Since different combinations of rings can result in strength enhancements, all ring characteristics were used. With R^2 values greater than 97.47, Practicing engineers can use these equations (Equations 11 and 12) to accurately predict the ultimate strength and the strength ratio to mitigate potential risks associated with structural failure and ensuring the longevity and efficiency of offshore structures.

c) The optimal outcomes with a maximum ultimate strength of 625.67kN and a maximum strength ratio of 2.64 with a maximum error of 1.7% show excellent accuracy.

6. Nomenclature

D	Chord diameter	d	Brace diameter
T	Chord thickness	t	Brace thickness
θ	Angle between the outer inclined brace and the chord	L	Chord length
H	Height of brace	g	Gap between central brace and outer angular brace
h_s	Height of the stiffener	t_s	Thickness of the stiffener
w_s	Distance between outer stiffener's center	β	Ratio of the diameter of brace and chord
γ	Ratio of chord's diameter and twice chord's thickness	τ	Ratio of brace thickness to chord thickness
ζ	Ratio of "gap between central and outer inclined brace" and diameter of the chord	α	Ratio of twice the length of the chord to the diameter of the chord
α_b	Ratio of twice the length of brace to the diameter of the brace	h_s	Difference between outer and inner diameters of internal rings
δ	Ratio of "difference between outer and inner diameters of internal rings" and diameter of the chord	ψ	Ratio of the thickness of rings to the thickness of the chord
λ	Product of the width of outer stiffener and spacing ratio "a."	P_{st}	Ultimate strength of stiffened joint
P_{ust}	Ultimate strength of unstiffened joint	Ω	Ratio of P_{st} and P_{ust}
SCF	Stress concentration factors	IRS	Internally ring-stiffened joints
RSM	Response surface methodology	ANOVA	Analysis of variance
R^2	Coefficient of determination	P-value	Significance level
S	Standard error of estimate	R-sq(adj)	Optimal balance between model, fit and quality
R-sq(Predicted)	Model's ability to assess new data	Dj value	Desirability value
$\beta_\circ$	Constant in quadratic predictive model	βi	Linear regression coefficient
∈	Random error component	βij	Coefficient for coupling terms
βii	Quadratic regression coefficient	FEA	Finite element analysis
x_i and x_j	Input variables		

7. Declarations

7.1. Author Contributions

Conceptualization, A.R. and S.K.; methodology, A.R. and S.K.; software, A.R. and M.I.; validation, A.R.; formal analysis, A.R.; investigation, A.R.; resources, S.K.; data curation, S.K. and A.R.; writing—original draft preparation, A.R.; writing—review and editing, A.R. and M.O.; visualization, A.R.; supervision, S.K., V.P., and M.O.; project administration, S.K. and V.P.; funding acquisition, S.K. All authors have read and agreed to the published version of the manuscript.

7.2. Data Availability Statement

The data presented in this study are available on request from the corresponding author.

7.3. Funding

This research received funding from Yayasan Universiti Teknologi PETRONAS under grant No. 015LC0-443.

7.4. Conflicts of Interest

The authors declare no conflict of interest.

8. References

[1] Yang, K., Zhu, L., Bai, Y., Sun, H., & Wang, M. (2018). Strength of external-ring-stiffened tubular X-joints subjected to brace axial compressive loading. Thin-Walled Structures, 133, 17-26. doi:10.1016/j.tws.2018.09.030.

[2] Dehghani, A., & Aslani, F. (2019). A review on defects in steel offshore structures and developed strengthening techniques. Structures, 20, 635–657. doi:10.1016/j.istruc.2019.06.002.

[3] Iqbal, M., Karuppanan, S., Perumal, V., Ovinis, M., & Rasul, A. (2023). Rehabilitation Techniques for Offshore Tubular Joints. Journal of Marine Science and Engineering, 11(2). doi:10.3390/jmse11020461.

[4] Choo, Y. S., Liang, J. X., Van Der Vegte, G. J., & Liew, J. Y. R. (2004). Static strength of collar plate reinforced CHS X-joints loaded by in-plane bending. Journal of Constructional Steel Research, 60(12), 1745–1760. doi:10.1016/j.jcsr.2004.05.005.

[5] Nassiraei, H., Mojtahedi, A., & Lotfollahi-Yaghin, M. A. (2018). Static strength of X-joints reinforced with collar plates subjected to brace tensile loading. Ocean Engineering, 161, 227–241. doi:10.1016/j.oceaneng.2018.05.017.

[6] Shao, Y. B. (2016). Static strength of collar-plate reinforced tubular T-joints under axial loading. Steel and Composite Structures, 21(2), 323–342. doi:10.12989/scs.2016.21.2.323.

[7] Nassiraei, H., Zhu, L., Lotfollahi-Yaghin, M. A., & Ahmadi, H. (2017). Static capacity of tubular X-joints reinforced with collar plate subjected to brace compression. Thin-Walled Structures, 119(June), 256–265. doi:10.1016/j.tws.2017.06.012.

[8] Feng, R., Chen, Y., & Chen, D. (2017). Experimental and numerical investigations on collar plate and doubler plate reinforced SHS T-joints under axial compression. Thin-Walled Structures, 110, 75–87. doi:10.1016/j.tws.2016.10.017.

[9] Rajić, A., Lukačević, I., Skejić, D., & Ungureanu, V. (2023). Cold-formed Steel-Concrete Composite Beams with Back-to-Back Channel Sections in Bending. Civil Engineering Journal, 9(10), 2345-2369. doi:10.28991/CEJ-2023-09-10-01.

[10] Choo, Y. S., Liang, J. X., Van Der Vegte, G. J., & Liew, J. Y. R. (2004). Static strength of doubler plate reinforced CHS X-joints loaded by in-plane bending. Journal of Constructional Steel Research, 60(12), 1725–1744. doi:10.1016/j.jcsr.2004.05.004.

[11] Gjukaj, A., Salihu, F., Muriqi, A., & Cvetanovski, P. (2023). Numerical Behavior of Extended End-Plate Bolted Connection under Monotonic Loading. HighTech and Innovation Journal, 4(2), 294-308. doi:10.28991/HIJ-2023-04-02-04.

[12] Gao, F., Tang, Z., Guan, X., Zhu, H., & Chen, Z. (2018). Ultimate strength of tubular T-joints reinforced with doubler plates after fire exposure. Thin-Walled Structures, 132(April), 616–628. doi:10.1016/j.tws.2018.09.021.

[13] Zavvar, E., Sadat Hosseini, A., & Lotfollahi-Yaghin, M. A. (2021). Stress concentration factors in steel tubular KT-connections with FRP-Wrapping under bending moments. Structures, 33(July), 4743–4765. doi:10.1016/j.istruc.2021.06.100.

[14] Lesani, M., Bahaari, M. R., & Shokrieh, M. M. (2014). Experimental investigation of FRP-strengthened tubular T-joints under axial compressive loads. Construction and Building Materials, 53, 243–252. doi:10.1016/j.conbuildmat.2013.11.097.

[15] Nassiraei, H., & Rezadoost, P. (2021). Stress concentration factors in tubular X-connections retrofitted with FRP under compressive load. Ocean Engineering, 229(April), 108562. doi:10.1016/j.oceaneng.2020.108562.

[16] Hosseini, A. S., Bahaari, M. R., & Lesani, M. (2020). SCF distribution in FRP-strengthened tubular T-joints under brace axial loading. Scientia Iranica, 27(3 A), 1113–1129. doi:10.24200/SCI.2018.5471.1293.

[17] Masilamani, R., & Nallayarasu, S. (2021). Experimental and numerical investigation of ultimate strength of ring-stiffened tubular T-joints under axial compression. Applied Ocean Research, 109, 102576. doi:10.1016/j.apor.2021.102576.

[18] Lee, M. M. K., & Llewelyn-Parry, A. (2005). Strength prediction for ring-stiffened DT-joints in offshore jacket structures. Engineering Structures, 27(3), 421–430. doi:10.1016/j.engstruct.2004.11.004.

[19] Lee, M. M. K., & Llewelyn-Parry, A. (1999). Strength of ring-stiffened tubular T-joints in offshore structures: A numerical parametric study. Journal of Constructional Steel Research, 51(3), 239–264. doi:10.1016/S0143-974X(99)00027-9.

[20] Lan, X., Wang, F., Ning, C., Xu, X., Pan, X., & Luo, Z. (2016). Strength of internally ring-stiffened tubular DT-joints subjected to brace axial loading. Journal of Constructional Steel Research, 125, 88–94. doi:10.1016/j.jcsr.2016.06.012.

[21] Li, Q., Zhou, X., Wang, Y., Lim, J. B. P., Wang, B., & Gao, S. (2024). Static performance of multi-planar CFST chord-CHS brace KK joints. Journal of Constructional Steel Research, 213, 108428. doi:10.1016/j.jcsr.2023.108428.

[22] Boretzki, J., Albiez, M., Myslicki, S., Vallée, T., & Ummenhofer, T. (2024). Hybrid grouted joints: Load bearing and failure behaviour under static, axial loading. Construction and Building Materials, 413, 134691. doi:10.1016/j.conbuildmat.2023.134691.

[23] Lin, G., Zeng, J., Li, J., & Chen, G. M. (2024). Chord axial compressive behavior of hybrid FRP-concrete-steel double-skin tubular member T-joints. Thin-Walled Structures, 196, 111535. doi:10.1016/j.tws.2023.111535.

[24] Ahmadi, H., & Lotfollahi-Yaghin, M. A. (2013). Experimental and numerical investigation of geometric SCFs in internally ring-stiffened tubular KT-joints of offshore structures. Journal of the Persian Gulf, 4(12), 1-12.

[25] Wimpey Offshore. (1991). In-service database for ring-stiffened tubular joints. Report WOL, 35, 91, London, United Kingdom.

[26] Azari Dodaran, N., Ahmadi, H., & Lotfollahi-Yaghin, M. A. (2018). Static strength of axially loaded tubular KT-joints at elevated temperatures: Study of geometrical effects and parametric formulation. Marine Structures, 61(June), 282–308. doi:10.1016/j.marstruc.2018.06.009.

[27] Sadat Hosseini, A., Zavvar, E., & Ahmadi, H. (2021). Stress concentration factors in FRP-strengthened steel tubular KT-joints. Applied Ocean Research, 108(September), 102525. doi:10.1016/j.apor.2021.102525.

[28] Iqbal, M., Karuppanan, S., Perumal, V., Ovinis, M., & Rasul, A. (2023). Numerical investigation of crack mitigation in tubular KT-joints using composite reinforcement. Engineering Proceedings, 56(1), 255. doi:10.3390/ASEC2023-16290.

[29] Ahmadi, H., Lotfollahi-Yaghin, M. A., & Yong-Bo, S. (2013). Chord-side SCF distribution of central brace in internally ring-stiffened tubular KT-joints: A geometrically parametric study. Thin-Walled Structures, 70, 93–105. doi:10.1016/j.tws.2013.04.011.

[30] Ahmadi, H., Ali Lotfollahi-Yaghin, M., Yong-Bo, S., & Aminfar, M. H. (2012). Parametric study and formulation of outer-brace geometric stress concentration factors in internally ring-stiffened tubular KT-joints of offshore structures. Applied Ocean Research, 38, 74–91. doi:10.1016/j.apor.2012.07.004.

[31] Ahmadi, H., & Lotfollahi-Yaghin, M. A. (2015). Stress concentration due to in-plane bending (IPB) loads in ring-stiffened tubular KT-joints of offshore structures: Parametric study and design formulation. Applied Ocean Research, 51, 54–66. doi:10.1016/j.apor.2015.02.009.

[32] Ahmadi, H., & Zavvar, E. (2015). Stress concentration factors induced by out-of-plane bending loads in ring-stiffened tubular KT-joints of jacket structures. Thin-Walled Structures, 91, 82–95. doi:10.1016/j.tws.2015.02.011.

[33] Kohnke, P. (2009). Theory reference for the mechanical APDL and mechanical applications. Ansys Inc, Pennsylvania, United States.

[34] Marshall, P. W. (2013). Design of welded tubular connections: Basis and use of AWS code provisions. Elsevier, Amsterdam, Netherlands.

[35] Zavvar, E., Hectors, K., & De Waele, W. (2021). Stress concentration factors of multi-planar tubular KT-joints subjected to in-plane bending moments. Marine Structures, 78. doi:10.1016/j.marstruc.2021.103000.

[36] Iskander, M. S., Shaat, A. A., Sayed-Ahmed, E. Y., & Soliman, E. A. (2017). Strengthening CHS T-joints subjected to brace axial compression using through-bolts. Journal of Constructional Steel Research, 128, 555–566. doi:10.1016/j.jcsr.2016.09.019.

[37] Wardenier, J., Kurobane, Y., Packer, J. A., Van der Vegte, G. J., & Zhao, X. L. (2008). Design guide for circular hollow section (CHS) joints under predominantly static loading. Cidect, Geneva, Switzerland.

[38] Swensson, K. D., & Yura, J. A. (1986). Stress Concentration Factors in Double-Tee Tubular Joints. PMFSEL Report No.

[39] Li, X., Zhang, L., Xue, X., Wang, X., & Wang, H. (2018). Prediction on ultimate strength of tube-gusset KT-joints stiffened by 1/4 ring plates through experimental and numerical study. Thin-Walled Structures, 123, 409–419. doi:10.1016/j.tws.2017.11.029.

[40] Qu, H., Li, A., Huo, J., & Liu, Y. (2017). Dynamic performance of collar plate reinforced tubular T-joint with precompression chord. Engineering Structures, 141, 555-570. doi:10.1016/j.engstruct.2017.03.037.

[41] Ahmadi, H., Yeganeh, A., Mohammadi, A. H., & Zavvar, E. (2016). Probabilistic analysis of stress concentration factors in tubular KT-joints reinforced with internal ring stiffeners under in-plane bending loads. Thin-Walled Structures, 99, 58–75. doi:10.1016/j.tws.2015.11.010.

[42] Efthymiou, M. (1988). Development of SCF formulae and generalized influence functions for use in fatigue analysis. OTJ 88. Recent Developments in Tubular Joints Technology, Surrey, United Kingdom.

[43] Khan, M. B., Iqbal Khan, M., Shafiq, N., Abbas, Y. M., Imran, M., Fares, G., & Khatib, J. M. (2023). Enhancing the mechanical and environmental performance of engineered cementitious composite with metakaolin, silica fume, and graphene nanoplatelets. Construction and Building Materials, 404(March), 133187. doi:10.1016/j.conbuildmat.2023.133187.

[44] Nassiraei, H. (2020). Local joint flexibility of CHS T/Y-connections strengthened with collar plate under in-plane bending load: parametric study of geometrical effects and design formulation. Ocean Engineering, 202, 107054. doi:10.1016/j.oceaneng.2020.107054.

[45] Karim, M. A., Abdullah, M. Z., Waqar, A., Deifalla, A. F., Ragab, A. E., & Khan, M. (2023). Analysis of the mechanical properties of the single layered braid reinforced thermoplastic pipe (BRTP) for oil & gas industries. Results in Engineering, 20, 101483. doi:10.1016/j.rineng.2023.101483.

Appendix I: Summary of ANOVA

Responses	Source	DF	Adj SS	Adj MS	F-Value	P-Value	Responses	Source	DF	Adj SS	Adj MS	F-Value	P-Value
Ultimate strength	Model	25	1350154	54006	3195.31	<0.001	Strength ratio	Model	22	13.5799	0.61727	969.21	0.000
	Linear	8	751641	93955	5558.92	<0.001		Linear	8	8.6336	1.07920	1694.52	<0.001
	β	1	51080	51080	3022.21	<0.001		β	1	2.6078	2.60780	4094.66	<0.001
	γ	1	509222	509222	30128.44	<0.001		γ	1	2.2396	2.23962	3516.56	<0.001
	τ	1	1298	1298	76.79	<0.001		τ	1	0.0785	0.07855	123.33	<0.001
	θ	1	138	138	8.17	0.005		θ	1	0.0023	0.00226	3.54	0.02
	ζ	1	4635	4635	274.25	<0.001		ζ	1	0.0249	0.02493	39.15	<0.001
	λ	1	453	453	26.78	<0.001		λ	1	0.0085	0.00848	13.31	<0.001
	δ	1	20140	20140	1191.59	<0.001		δ	1	0.8238	0.82377	1293.46	<0.001
	ψ	1	22788	22788	1348.26	<0.001		ψ	1	0.3163	0.31629	496.62	<0.001
	Square	5	11862	2372	140.36	<0.001		Square	3	0.1020	0.03400	53.39	<0.001
	β*β	1	273	273	16.15	<0.001		ζ*ζ	1	0.0147	0.01468	23.05	<0.001
	γ*γ	1	4466	4466	264.25	<0.001		λ * λ	1	0.0431	0.04311	67.69	<0.001
	ζ*ζ	1	624	624	36.92	<0.001		ψ * ψ	1	0.0442	0.04421	69.42	<0.001
	λ * λ	1	2857	2857	169.06	<0.001		2-Way Interaction	11	0.9376	0.08523	133.83	<0.001
	ψ * ψ	1	2975	2975	176.04	<0.001		β* λ	1	0.0051	0.00513	8.05	0.005
	2-Way Interaction	12	40497	3375	199.67	<0.001		β* δ	1	0.1941	0.19413	304.82	<0.001
	β* λ	1	220	220	13.00	<0.001		β* ψ	1	0.0570	0.05699	89.48	<0.001
	β* δ	1	9886	9886	584.91	<0.001		γ* λ	1	0.0049	0.00494	7.75	0.006
	β* ψ	1	3123	3123	184.76	<0.001		γ* δ	1	0.1192	0.11916	187.10	<0.001
	γ* δ	1	1242	1242	73.48	<0.001		γ* ψ	1	0.0788	0.07879	123.72	<0.001
	τ* λ	1	296	296	17.53	<0.001		τ* λ	1	0.0037	0.00371	5.83	0.017
	τ* δ	1	97	97	5.75	0.018		ζ* δ	1	0.0156	0.01564	24.56	<0.001
	ζ* λ	1	154	154	9.12	0.003		λ * δ	1	0.1679	0.16794	263.70	<0.001
	ζ* δ	1	792	792	46.87	<0.001		λ * ψ	1	0.0453	0.04533	71.18	<0.001
	ζ* ψ	1	72	72	4.23	0.041		δ * ψ	1	0.1172	0.11717	183.97	<0.001
	λ * δ	1	12066	12066	713.88	<0.001							
	λ * ψ	1	3095	3095	183.10	<0.001							
	δ * ψ	1	9338	9338	552.51	<0.001							